JOURNAL OF SPACECRAFT AND ROCKETS
Vol. 47, No. 2, March–April 2010

Electrodynamic Tethers Under Forced-Current Variations Part 1: Periodic Solutions for Tether Librations

Paul Williams*
Delft University of Technology, 2629 HS Delft, The Netherlands

DOI: 10.2514/1.45731

Varying the current in electrodynamic tethers provides a means for manipulating the orbits of spacecraft. These variations can induce unstable librational motion of the tether. Periodic solutions of electrodynamic tethers under forced currents are studied, which provide a reference trajectory for feedback control of the tether librations during orbit transfer. The tether is treated as a dumbbell, and periodic solutions are obtained by means of the Legendre pseudospectral method. The technique provides the stability characteristics of the solutions by application of Floquet's theory. Five different current profiles suitable for orbital maneuvering are used to obtain periodic solutions. An energy-rate feedback controller is applied to stabilize the dumbbell librations around the time-varying reference trajectory. The results show that sinusoidal and cosine currents with frequencies equal to that of the orbit are neutrally stable for some orbit inclinations, whereas a cosine current with frequency twice that of the orbit is unstable, with the degree of instability growing with the current amplitude.

Nomenclature

$D_{k,j}$	=	differentiation matrix row k, column j
E	=	nondimensional energy flux
I	=	electric current, A
i	=	orbit inclination, deg
k_1	=	feedback gain
L_N	=	Nth-order Legendre polynomial
l	=	tether length, km
m_s	=	subsatellite mass, kg
m_t	=	tether mass, kg
N	=	number of nodes used in pseudospectral method
t	=	dimensional time, s
$\boldsymbol{u}$	=	control input vector
w_j	=	jth Gauss–Lobatto weight
$\boldsymbol{x}$	=	state vector
ε	=	amplitude of nondimensional current
$\bar{\varepsilon}$	=	nondimensional current
θ	=	in-plane libration angle, deg
λ	=	eigenvalue of monodromy matrix
μ	=	Earth's gravitational parameter, m^3/s^2
μ_m	=	magnetic field dipole strength, N/A
ν	=	true anomaly, rad
τ	=	computational domain used in pseudospectral method
ϕ	=	out-of-plane libration angle, deg
$\phi_j(t)$	=	jth Lagrange interpolating polynomial
ω	=	orbital angular velocity, rad/s

Subscript

ref	=	reference periodic solution

Superscript

$'$	=	$\mathrm{d}/\mathrm{d}(\omega t)$

Received 30 May 2009; revision received 12 October 2009; accepted for publication 15 October 2009.

*Currently RMIT University, 1/4 Maylands Avenue, Balwyn North, VIC 3104, Australia; tethered.systems@gmail.com. Member AIAA.

I. Introduction

ELECTRODYNAMIC tethers are expected to be a viable and efficient means for generating power or controlling the orbit of future spacecraft [1–5]. The electric current flowing in the tether generates a Lorentz force perpendicular to the local tether direction and the magnetic field vector. By controlling the direction and magnitude of the current in the tether, it is possible to alter the orbital elements in a controlled manner. Because of the relatively low currents involved, it takes long periods of time to affect significant changes to the spacecraft orbit.

In electrodynamic tether systems, the tether can be either bare or insulated. A bare tether allows electrons to be collected along the tether length, whereas an insulated tether requires a dedicated anodic collector, which results in a constant current along the tether length. Consequently, a bare tether does not have a constant current along the tether length. For many proposed applications, such as deorbit, the current is required to flow only in one direction. However, control of the evolution of all of the orbital elements requires the ability to reverse the current direction in the tether. This can only be achieved by using an onboard power source. Thus, a distinction must be made between simpler one-way electrodynamic tethers and those that require more complex reversible currents. In this paper, electrodynamic tether systems with forced reversible currents are considered. These types of currents are optimal for large-scale orbital maneuvering.

One of the challenges in electrodynamic tether control is the coupling between the electric current and tether librations. The libration state changes on a faster time scale compared with the orbital elements, and the lateral tether dynamics change on an even faster time scale. Since the orbital forces are a function of the tether orientation in space, it is clear that the librational modes couple to the orbital maneuvering forces. One way of mitigating the effects of librations is to take them into account in the trajectory planning. However, this can be difficult due to the chaotic nature of librations in elliptic orbits [6]. The problem is compounded by the fact the librational dynamics are unstable under application of a constant current [7]. Instability of librations can lead to very large libration amplitudes or even tumbling of the entire system. Instability of the librations does not necessarily imply that the system will always begin tumbling, and the amplitude of libration oscillations is strongly dependent on the current amplitude, degree of instability, and orbital parameters. However, even if the librations themselves are bounded, they may be difficult to predict and hence can play a significant role in the evolution of the orbital trajectory. One possible means for stabilizing the librations is to use the periodic solutions for the librations as a reference and to superimpose a current correction on

the mission current to stabilize the librations around the reference. This approach was considered in [8] for the case of a constant reference current using nonlinear feedback of the librational energy rate. Constant currents are applicable for changing the semimajor axis, but time-varying currents are required for controlling the other orbital elements.

Periodic solutions are the proper reference trajectory for stabilizing electrodynamic tethers because they represent the ideal case of zero net rotational energy input per orbit [9]. The periodic solution is unstable, with instability growing with the electric current [7]. Periodic solutions have also been determined for tethers, including the lateral dynamics [10]. The instability in the lateral dynamics grows at a faster rate than the librational instability. The effect of orbit eccentricity was shown by Peláez and Andres [11] to amplify the unstable nature of the dynamics. Corsi and Iess [12] considered a simple control scheme to stabilize the tether librations for deorbiting applications. Hoyt [13] has described schemes for stabilizing flexible electrodynamic tethers during deorbit by periodically measuring the motion of several points along the tether to estimate the oscillation energy and adjusting the control input accordingly. The application of electromagnetic forces for directly controlling the librational motion has also been considered [14–17]. Takeichi [18] suggested using a switching control function to help stabilize the tether librations during deorbit, whereas Lanoix et al. [19] employed a sinusoidal current at 3 times the orbital frequency superimposed on a constant current to help bound out-of-plane librations during deorbit. Control of the unstable skip-rope motion during retrieval was shown to be effectively suppressed by Williams et al. [17] if a movable attachment point is used to damp the lateral oscillations of the electrodynamic tether. Peláez and Lorenzini [20] addressed the issue of controlling the librations of an electrodynamic tether around the periodic solution. Their approach consisted of two linear feedback-control schemes. The first was simple proportional feedback for the in- and out-of-plane libration rates, and the second was a delayed-feedback version of the same controller. However, the implementations of these controllers were assumed to be independent, where it was suggested that control could be achieved using movement of the tether attachment point. For the case of a constant current, Williams [8] used an energy-rate feedback approach to stabilize the librational motion of the tether around the periodic solution by adjusting the amount of current flowing in the tether. More recently, Williams [21] used a predictive control implementation using time-delayed feedback of the tether librational states to stabilize the tether librations in the absence of a reference trajectory.

The case of a constant-current input provides a good reference from which to work if it is not desired to control the evolution of the orbital elements with more precision. Tragesser and San [22] developed a guidance algorithm for maneuvering hanging electrodynamic tethers between arbitrary orbits (restricted, however, to nonzero eccentricities because of the restrictions imposed by the perturbation equations). In their approach, the tether librations were neglected and control of the orbital elements was achieved by determining the variation in current to produce secular changes in each of the orbital elements. This approach was extended to the case of spinning tethers in [23]. In these cases, the required electric current can vary considerably during the course of an orbit. Hence, it is desirable to determine the nature of any possible periodic solutions for the tether librations for the case in which the prescribed variation in current is also periodic. If the periodic solutions for forced currents are known, then these can be used to improve the accuracy of long-term guidance schemes. Some preliminary work in this area has been made by Sabey and Tragesser [24].

This paper is the first of a two-part paper that investigates the effects of forced currents on the behavior of electrodynamic tethers. In this paper, periodic solutions are obtained for the case of time-varying reference currents. In [8,9,11] periodic solutions for inelastic electrodynamic tethers were obtained for the case of a constant-current input using the Poincaré continuation method [25]. Unfortunately, this algorithm was found to be unstable for the case of forced-current variations and so an approach based on the Legendre pseudospectral method is used in this work [26]. This method is fast, efficient and provides stability information from the discretized Jacobian. An energy-rate control law is applied and shown to stabilize the librations. In Part 2 [27], the results are extended to consider flexible tethers, where estimates of the tether shape are used in the feedback controller for stabilizing the librations and lateral vibrations simultaneously.

II. Mathematical Model

In this work, a simplified tether model is used for studying the librational dynamics of an electrodynamic tether system under forced-current variations. In Part 2 [27], a discretized tether model that accounts for the tether lateral flexibility is introduced. However, preliminary investigations into stability and control of librations can be made using the so-called dumbbell model. The dumbbell model of the tether is adopted from Peláez and Lorenzini [20]. In the dumbbell model, two point masses are assumed to be connected by an inelastic rigid rod. By assumption in this work, the perturbing forces created by electrodynamic forces do not influence the orbital motion of the system. This implies that the mother satellite is sufficiently large in mass compared with the subsatellite and tether so that the system center of mass can be considered to coincide with that of the mother satellite. Hence, the mother satellite is assumed to remain in a circular orbit, and the tether is modeled by a rigid rod undergoing forced librations due to the electric current. For more generality, the nondimensional parameter $\bar{\varepsilon} = f_e I \mu_m / \mu(m_s + m_t/3)$ is used, where f_e is a parameter governing the distribution of electric current along the tether, I is the current, μ_m is the magnetic field strength, μ is the gravitational constant of the Earth, m_s is the subsatellite mass, and m_t is the tether mass. Essentially, the parameter $\bar{\varepsilon}$ governs the ratio of torque due to electrodynamics to the torque due to gravitational forces.

Under these assumptions, the kinetic and potential energy of the tether in a circular orbit are given, respectively, by

$$\mathcal{T} = \tfrac{1}{2}(m_s + m_t/3)\omega^2 l^2[\phi'^2 + (\theta' + 1)^2\cos^2\phi] \tag{1}$$

$$\mathcal{V} = -\tfrac{3}{2}\omega^2(m_s + m_t/3)l^2\cos^2\theta\cos^2\phi \tag{2}$$

where $' = \mathrm{d}/\mathrm{d}(\omega t)$ is the nondimensional time derivative. The application of Lagrange's equations leads to the equations of motion:

$$\theta'' = 2(\theta' + 1)\phi' \tan\phi - 3\sin\theta\cos\theta - \bar{\varepsilon}[\sin i \tan\phi(2\sin\nu\cos\theta - \cos\nu\sin\theta) + \cos i] \tag{3}$$

$$\phi'' = -\sin\phi\cos\phi[(\theta' + 1)^2 + 3\cos^2\theta] + \bar{\varepsilon}(2\sin\nu\sin\theta + \cos\nu\cos\theta)\sin i \tag{4}$$

The generalized forces appearing in Eqs. (3) and (4) and are derived elsewhere [20]. The main assumption used in the derivation of the equations of motion is that the magnetic field is represented by a nontilted dipole. A tilted dipole introduces a long-term secular effect into the response, which is not treated here. The secular effect is time dependent, and hence it is not possible to determine common periodic solutions to be used as reference trajectories if a tilted dipole model is used. The following section describes the numerical algorithm for determining periodic solutions to the governing equations of motion.

III. Feedback Controller

In [8], energy-rate feedback was demonstrated for tracking the periodic trajectory of an electrodynamic tether using current control. The case demonstrated in [8] was for a constant reference current. Here, it will be shown that the feedback controller works equally well

for the case of a nonconstant reference current, such as those used to manipulate the orbital elements in a controlled manner [22].

A feedback controller is proposed of the following form:

$$\bar{\varepsilon} = \bar{\varepsilon}_{\text{ref}}[1 - k_1(E - E_{\text{ref}})\text{sign}\bar{\varepsilon}_{\text{ref}}] \tag{5}$$

where k_1 is a feedback gain, and

$$\begin{aligned} E_{\text{ref}} &= \phi'_{\text{ref}}(2\sin\nu\sin\theta_{\text{ref}} + \cos\nu\cos\theta_{\text{ref}})\sin i \\ &\quad - [\sin i\tan\phi_{\text{ref}}(2\sin\nu\cos\theta_{\text{ref}} - \cos\nu\sin\theta_{\text{ref}}) \\ &\quad + \cos i]\theta'_{\text{ref}}\cos^2\phi_{\text{ref}} \end{aligned} \tag{6}$$

is the reference librational energy flux. Note that the controller defined by Eq. (5) is different from the one in [8]. The controller used in this paper has been simplified slightly. The controller uses the measured librational energy flux E,

$$\begin{aligned} E &= \phi'(2\sin\nu\sin\theta + \cos\nu\cos\theta)\sin i \\ &\quad - [\sin i\tan\phi(2\sin\nu\cos\theta - \cos\nu\sin\theta) + \cos i]\theta'\cos^2\phi \end{aligned} \tag{7}$$

and corrects the reference current with a term proportional to the error in the energy flux. The selection of the control gain k_1 and stability of the controller are determined by means of Floquet's theory.

IV. Forced Currents

Carroll [28] specified five different current variations that can be used to change the orbital elements using electrodynamic tethers. These are 1) constant current, 2) sinusoidal current at the orbital frequency as a function of true anomaly, 3) cosine current at the orbital frequency as a function of true anomaly, 4) sinusoidal current at twice the orbital frequency as a function of true anomaly, and 5) cosine current at twice the orbital frequency as a function of true anomaly. The case of a constant current has received the most focus in the literature and is chiefly responsible for altering the orbit semimajor axis. A sinusoidal current can be used to alter the argument of perigee. A cosine current can be used to alter the orbit eccentricity. A sinusoidal current at twice the orbital frequency can be used to alter the longitude of the ascending node. A cosine current at twice the orbital frequency can be used to alter the orbit inclination. The generation of periodic solutions for the last four current variations is the focus of this work. In addition to these, a superposition of a constant current and forced current is also considered. One of the limitations of the work presented here is that only circular orbits are considered. Elliptical orbits introduce additional complexities that should be dealt with in future work.

V. Numerical Algorithm

The algorithm used to compute periodic solutions in this work is based on direct transcription methods. These methods are typically used for optimal control problems because of their reduced sensitivity compared with shooting-type methods. There are a variety of direct transcription methods in the literature, and one of the most important is the Legendre pseudospectral method [29,30]. This method has some theoretical advantages compared with other similar techniques, but more important, it is able to provide stability information about the periodic solutions with very little additional labor. This has been explained in [26] and is summarized in the following section.

A. Legendre Pseudospectral Method

Consider the problem of finding a periodic trajectory

$$\boldsymbol{x}(\boldsymbol{p}, t) = \boldsymbol{x}(\boldsymbol{p}, t + T)$$

and possibly the corresponding control input

$$\boldsymbol{u}(\boldsymbol{p}, t) = \boldsymbol{u}(\boldsymbol{p}, t + T)$$

and initial and final times t_0 and t_f ($T = t_f - t_0$) such that the cost function

$$J = \int_{t_0}^{t_f} \mathcal{L}[\boldsymbol{x}(t), \boldsymbol{u}(t), \boldsymbol{p}, t_0, t_f, t]\,\mathrm{d}t \tag{8}$$

is minimized subject to the dynamical constraints

$$\dot{\boldsymbol{x}}(t) = \boldsymbol{f}[\boldsymbol{x}(t), \boldsymbol{u}(t), \boldsymbol{p}, t], \qquad t \in [t_0, t_f] \tag{9}$$

and periodicity constraints

$$\boldsymbol{x}(t_0) = \boldsymbol{x}(t_f), \qquad \boldsymbol{u}(t_0) = \boldsymbol{u}(t_f) \tag{10}$$

where $\boldsymbol{x}(t) \in \mathbb{R}^{n_x}$ are the states, $\boldsymbol{u}(t) \in \mathbb{R}^{n_u}$ are the controls, $\boldsymbol{p} \in \mathbb{R}^{n_p}$ is a vector of parameters on which the periodic solution depends,

$$\mathcal{L} : \mathbb{R}^{n_x} \times \mathbb{R}^{n_u} \times \mathbb{R}^{n_p} \times \mathbb{R} \times \mathbb{R} \times \mathbb{R} \to \mathbb{R}$$

is the integrand of the selected cost function, and $t \in \mathbb{R}$ is the time. Although considered elsewhere [31–33] but not here, it is also possible to apply path constraints and general bounding box constraints to the formulation.

The problem is converted into a parameter optimization problem, in the case in which the cost function (8) and controls are nonzero, or a root-finding problem, in the case in which natural periodic solutions are sought. The Legendre pseudospectral method is applied for this purpose. The states and controls are expanded based on Lagrange interpolating polynomials:

$$\boldsymbol{x}^N(t) \approx \sum_{j=0}^{N} \boldsymbol{x}_j\phi_j(t), \qquad \boldsymbol{u}^N(t) \approx \sum_{j=0}^{N} \boldsymbol{u}_j\phi_j(t) \tag{11}$$

The coefficients $\boldsymbol{x}_j = \boldsymbol{x}(t_j)$ and $\boldsymbol{u}_j = \boldsymbol{u}(t_j)$ in Eq. (11) are the values of the states and controls at the Legendre–Gauss–Lobatto (LGL) points, which are the zeros of the derivative of the Nth-order Legendre polynomial L_N defined on the interval $\tau \in [-1, 1]$. The Lagrange interpolating polynomials are defined by

$$\phi_j(\tau) = \frac{(\tau^2 - 1)\dot{L}_N(\tau)}{(\tau - \tau_j)N(N+1)L_N(\tau_j)}, \qquad j = 0, \ldots, N \tag{12}$$

The state derivatives are approximated by analytically differentiating Eq. (11) and evaluating the result at the LGL points with the result expressible in terms of the differentiation matrix $\boldsymbol{D}$, for which the components are defined by

$$D_{k,j} := \begin{cases} \frac{L_N(\tau_k)}{L_N(\tau_j)}\frac{1}{(\tau_k - \tau_j)} & k \neq j \\ -\frac{N(N+1)}{4} & k = j = 0 \\ \frac{N(N+1)}{4} & k = j = N \\ 0 & \text{otherwise} \end{cases} \tag{13}$$

The derivatives of the states at the collocation points are easily expressed by the following relationship:

$$\dot{\widehat{\boldsymbol{x}}} \approx \frac{1}{\xi}\boldsymbol{D}\widehat{\boldsymbol{x}} \tag{14}$$

where $\widehat{\boldsymbol{x}} \triangleq [\boldsymbol{x}_0, \ldots, \boldsymbol{x}_N]$ is the discretized state vector across all nodes, and ξ is the transformation metric defined by the relationship between the computational domain τ and the physical time domain t:

$$t = (t_f - t_0)\tau/2 + (t_0 + t_f)/2 \tag{15}$$

$$\xi \triangleq \frac{\mathrm{d}t}{\mathrm{d}\tau} = (t_f - t_0)/2 \tag{16}$$

Finally, the integral cost function is discretized via a Gauss–Lobatto quadrature rule so that

$$\int_{t_0}^{t_f} \mathcal{L}(t)\,\mathrm{d}t = \xi \int_{-1}^{1} \mathcal{L}(t(\tau))\,\mathrm{d}\tau \approx \xi \sum_{j=0}^{N} w_j \mathcal{L}(t_j) \tag{17}$$

where w_j are the Legendre–Gauss–Lobatto weights defined by

$$w_j = \frac{2}{N(N+1)} \frac{1}{[L_N(\tau_j)]^2}, \qquad j = 0, \ldots, N \tag{18}$$

For further details of the method, as well as its application to optimal control problems, please see [29,30]. Thus, the discretized constraint equations given by Eqs. (9) and (10) are expressed by

$$\frac{1}{\xi} \sum_{j=0}^{N} D_{k,j} \boldsymbol{x}_j - \boldsymbol{f}[\boldsymbol{x}_k, \boldsymbol{u}_k, \boldsymbol{p}, t_k] = \boldsymbol{0}, \qquad k = 0, \ldots, N \tag{19}$$

$$\boldsymbol{x}_0 - \boldsymbol{x}_N = \boldsymbol{0}, \qquad \boldsymbol{u}_0 - \boldsymbol{u}_N = \boldsymbol{0} \tag{20}$$

In essence, because we are seeking smooth periodic solutions, the discretization converges at a spectral rate. The convergence of the method is understood from the point of view of a Sobolev space, denoted by $W^{m,p}(\Omega, \mathbb{R})$, which consists of all functions $f\colon \mathbb{R} \supseteq \Omega \to \mathbb{R}$ for which the jth derivative is in L^p for all $0 \le j \le m$, and L^p represents the standard L^p-norm. The method converges according to the theorem proved in [34].

B. Stability Computations

An effective method of computing the stability of the periodic solution is to use Floquet's theory on the variational equations derived by perturbing the periodic solution [35]:

$$\delta\dot{\boldsymbol{x}}(t) = [\boldsymbol{A}(t)]\delta\boldsymbol{x}(t) \tag{21}$$

where $A_{k,j} \triangleq \partial f_k / \partial x_j$ are continuous periodic functions with period T and are the elements of the matrix $[\boldsymbol{A}(t)]$. Equations (21) are linear and homogeneous. Floquet's theory gives the stability properties of the periodic solution as a function of the eigenvalues λ_i $(i = 1, \ldots, n_x)$ of the monodromy matrix $[M]$. Let $[\varphi(t)]$ be a fundamental matrix of Eq. (21), then any solution of Eq. (21) can be written as

$$\delta\boldsymbol{x}(t) = [\varphi(t)]\delta\boldsymbol{x}_0 \tag{22}$$

Consequently, the monodromy matrix is determined by letting $[\varphi(t_0)] = \mathbf{I}_{n_x \times n_x}$ to obtain $[M] = [\varphi(T)]$. Practically, the monodromy matrix is often computed by carrying out n_x integrations of Eq. (21) with initial conditions corresponding to the jth column of $\mathbf{I}_{n_x \times n_x}$ $(j = 1, \ldots, n_x)$. The algorithm presented by Lara and Peláez [25] uses the variational Eqs. (21) to compute the corrections to the periodic solution, and hence the monodromy matrix is automatically available to compute stability properties. If all the eigenvalues of the monodromy matrix satisfy $|\lambda_i| \le 1$ $(i = 1, \ldots, n_x)$, then the periodic solution is asymptotically stable. However, if any one of the eigenvalues has $|\lambda_i| > 1$, then the periodic solution is unstable. The procedure for obtaining the monodromy matrix using the Legendre pseudospectral (PS) method is given in [26] and summarized in the Appendix.

One of the main advantages of using Legendre PS method for obtaining periodic solutions is that no propagation of equations of motion is necessary, and hence sensitivity problems are not encountered. In addition, no continuation is necessary to obtain solutions due to global convergence of many nonlinear programming (NLP) problems including SNOPT [36]. However, if tracing the path of a particular family of solutions is desirable, continuation can still be applied by using a previous solution as the initial guess and applying a perturbation to the vector of parameters $\boldsymbol{p}$. In this case, much larger continuation steps can be taken than conventional algorithms.

VI. Numerical Results

In this section, numerical results are generated for different current profiles. Periodic solutions are sought only for the case in which the period is equal to the orbital period. Since we are interested in pure periodic solutions with a prescribed nondimensional current, the cost function in Eq. (8) is implemented with $J = 0$. This effectively reduces the NLP to a root-finding problem. The numerical results in this paper were generated using MATLAB with $N = 80$, and tolerances of 10^{-6} for feasibility and optimality were used in SNOPT. Feedback-control results were obtained using a fourth-order Runge–Kutta algorithm with error tolerances of 10^{-7}. Piecewise Hermite cubic-spline interpolation was used to interpolate the reference trajectory.

A. Sinusoidal Input at Orbital Frequency

Figure 1 shows the moduli of the eigenvalues of the monodromy matrix for the case in which the current variation is prescribed as $\bar{\varepsilon} = \varepsilon \sin \nu$ and the inclination is fixed at $i = 25$ deg. Figure 1 shows that the moduli of all of the eigenvalues are equal to 1 in the range plotted, except for in the interval of $\varepsilon \approx (1.025, 1.05)$. This suggests that the system is linearly stable, except in the range of $\varepsilon \approx (1.025, 1.05)$. This is a very promising because the librations of rigid electrodynamic tethers for the case of a constant current are known to be unstable. Hence, the librations of some forced-current inputs do not necessarily continue to pump energy into the librations when disturbed. Figure 2 shows examples of the periodic solutions on the θ–ϕ phase plane. For small values of ε, the periodic solutions are principally in the out-of-plane direction, with a very small in-plane component. For example, for the case of $\varepsilon = 0.1$, the peak out-

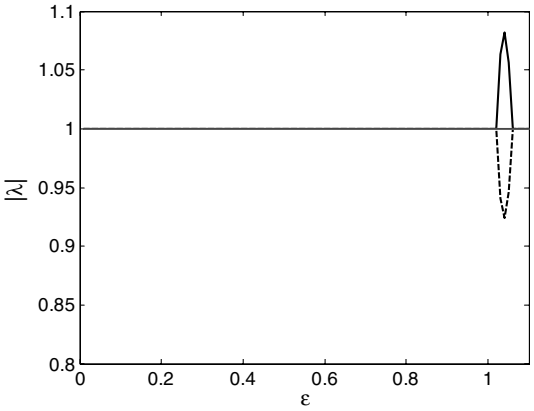

Fig. 1 Moduli of eigenvalues of monodromy matrix for $\bar{\varepsilon} = \varepsilon \sin \nu$, and $i = 25$ deg; λ_1 (thick black line), λ_2 (thin black line), λ_3 (thick gray line), and λ_4 (dashed line).

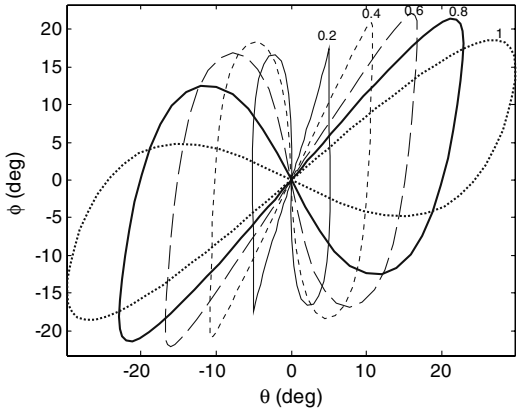

Fig. 2 Tether librations on phase plane for increasing ε for $\bar{\varepsilon} = \varepsilon \sin \nu$ and $i = 25$ deg (values of ε shown in plot).

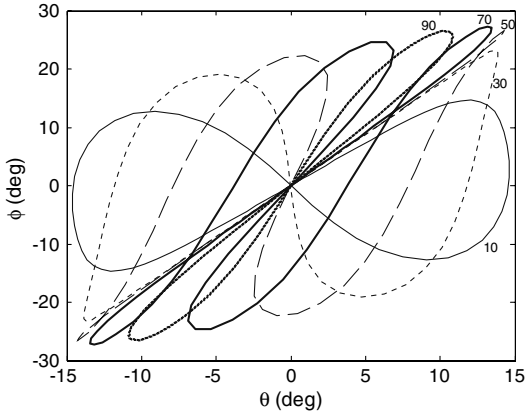

Fig. 3 Effect of inclination on $\bar{\varepsilon} = 0.5 \sin \nu$, shown at 20 deg increments for $0 < i < 90$ deg (values of i shown in plot).

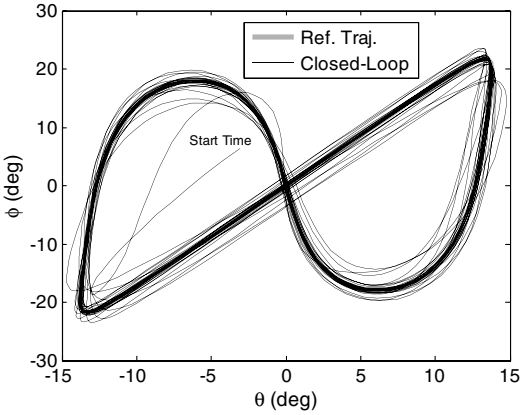

Fig. 5 Example of closed-loop control of tether librations under forced-current variations ($\bar{\varepsilon}_{\text{ref}} = 0.5 \sin \nu$, $k_1 = 4$, and $i = 25$ deg).

of-plane angle is approximately 14 deg, compared with a peak in-plane angle of approximately 2.7 deg. As the amplitude of the current increases, the in-plane motion begins to dominate the periodic solutions. For example, for $\varepsilon = 1.1$, the peak out-of-plane angle is approximately 15.76 deg, whereas the in-plane angle reaches approximately 34.6 deg. All of the periodic solutions are anti-symmetric about $\theta = 0$. Figure 3 shows results for variations in the orbital inclination in the range of $0 < i < 90$ deg for the current profile $\bar{\varepsilon} = 0.5 \sin \nu$. Note that all of these solutions appear linearly stable from the Floquet analysis, and hence the moduli of the eigenvalues of the monodromy matrix are not shown. Note that for $i = 0$, the periodic solution consists of libration purely in the orbital plane. This is due to the assumption of a nontilted dipole model of the magnetic field. The shape of the periodic solution can be seen to change quite dramatically as the orbit inclination increases. For small inclinations, the periodic solution exhibits a large peak-to-peak excursion in orbital plane and mild variation out of the orbit plane. The trajectories resemble a figure eight on its side. As the inclination increases, the out-of-plane dynamics begin to dominate the periodic solution, and the peak-to-peak variation in the in-plane librations decreases. For $i = 90$ deg, the periodic solution has a period of one-half of an orbit, due to the variation of current changing precisely with the direction of the magnetic field during the orbit. Again, this is a consequence of assuming a nontilted dipole.

The energy-rate feedback-controller stability was assessed for the inclination $i = 25$ deg, using k_1 as a continuation parameter. The monodromy matrix was formed using different values of k_1, with the periodic solution held fixed. Figure 4 shows a contour plot of the maximum magnitude of the eigenvalues of the monodromy matrix as a function of the current amplitude and feedback gain. This gives a direct measure of the controller stability. The plot shows that for $\varepsilon < 0.45$, the controller is stable for all control gains in the range of $0 < k_1 \leq 5$. For higher currents, the controller requires control gains larger than approximately 2.0 for the controller to yield stable solutions.

Figure 5 shows an example of the effectiveness of the feedback controller to provide closed-loop control of the electrodynamic tether under forced-current variations. The case selected uses the reference current $\bar{\varepsilon} = 0.5 \sin \nu$ at an inclination of $i = 25$ deg and a control gain of $k_1 = 4.0$. A random initial perturbation is applied to the periodic solution in Fig. 5, and the reference trajectory is also shown for clarity. The results clearly illustrate the convergence of the closed-loop trajectory to the reference one. Figure 6 shows the corresponding nondimensional current control input. Figure 6a shows the total nondimensional current, which is the superposition of the reference current and the feedback current. Figure 6b shows purely the feedback current. This illustrates that the major variations in the current are near the initial time with corrections on the order of 20% of the amplitude of the reference nondimensional current. The results show that the main disturbances are damped in approximately 25 orbits of the system.

B. Cosine Input at Orbital Frequency

Figure 7 shows the moduli of the eigenvalues of the monodromy matrix for the case in which the current variation is prescribed as $\bar{\varepsilon} = \varepsilon \cos \nu$ and the inclination is fixed at $i = 25$ deg. Figure 7 shows that the moduli of all of the eigenvalues are equal to 1 in the range plotted, except for in the interval of $\varepsilon \approx (0.875, 0.955)$,

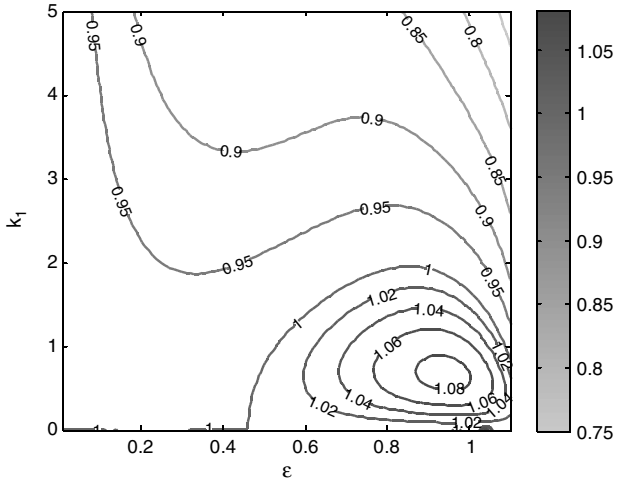

Fig. 4 Contours of maximum magnitude of the eigenvalues of the monodromy matrix for energy-rate feedback control with $\bar{\varepsilon} = \varepsilon \sin \nu$ and $i = 25$ deg.

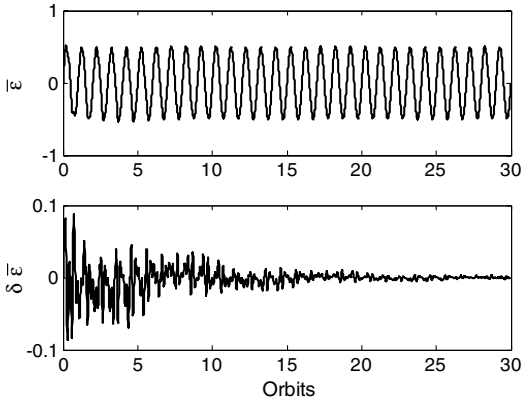

Fig. 6 Closed-loop control of tether librations under forced-current variations, showing a) total nondimensional current, and b) nondimensional current corrections due to feedback ($\bar{\varepsilon}_{\text{ref}} = 0.5 \sin \nu$, $k_1 = 4$, and $i = 25$ deg).

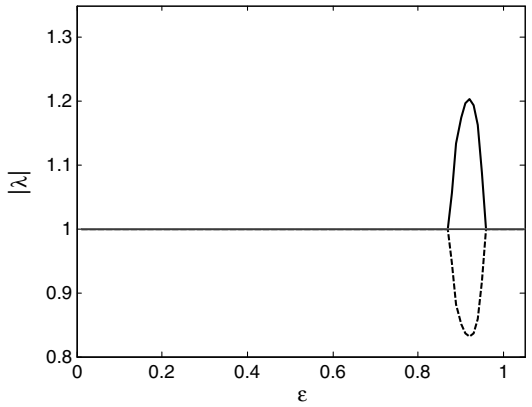

Fig. 7 Moduli of eigenvalues of monodromy matrix for $\bar{\varepsilon} = \varepsilon \cos \nu$, and $i = 25$ deg;λ_1 (thick black line), λ_2 (thin black line), λ_3 (thick gray line), and λ_4 (dashed line).

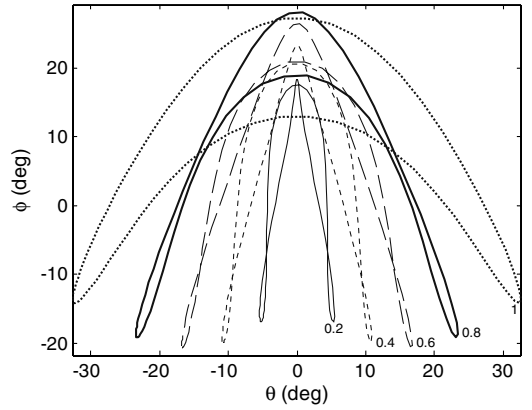

Fig. 8 Tether librations on phase plane for increasing ε for $\bar{\varepsilon} = \varepsilon \cos \nu$ and $i = 25$ deg (values of ε shown in plot).

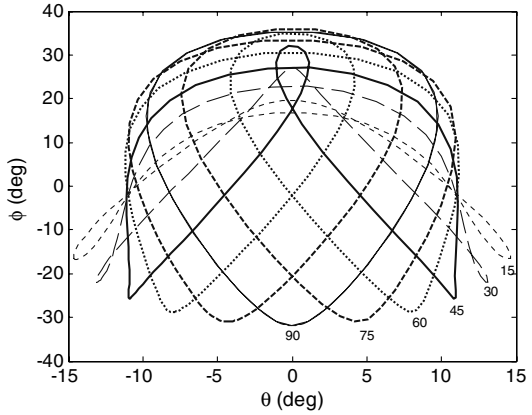

Fig. 9 Effect of inclination on $\bar{\varepsilon} = 0.5 \cos \nu$, shown at 15 deg increments for $0 < i < 90$ deg (values of i shown in plot).

suggesting that the system is linearly stable, except in the range of $\varepsilon \approx (0.875, 0.955)$. Figure 8 shows examples of the periodic solutions on the θ–ϕ phase plane, which illustrate that for low values of ε, the librations are principally out-of-plane librations. As ε increases, the in-plane libration amplitude of the solutions increases and the out-of-plane component becomes principally positive. The peak-to-peak variation of the out-of-plane component reduces as ε increases. In contrast to the case of a constant current, the periodic solutions are symmetric about the local vertical and asymmetric about the orbit plane for the out-of-plane librations. Figure 9 shows results for variations in the orbital inclination in the range of $0 <$

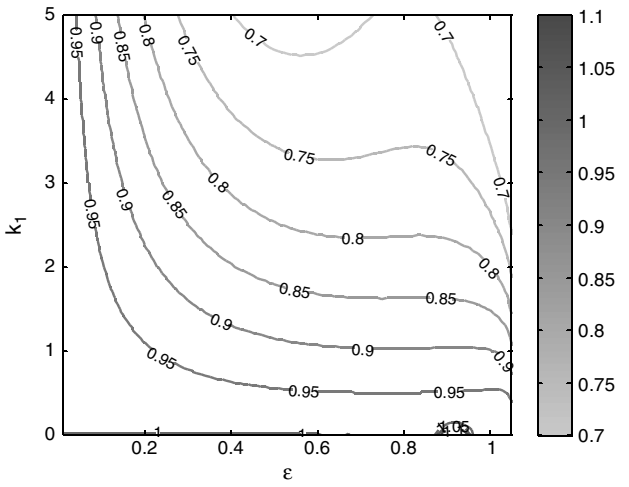

Fig. 10 Contours of maximum magnitude of the eigenvalues of the monodromy matrix for energy-rate feedback control with $\bar{\varepsilon} = \varepsilon \cos \nu$ and $i = 25$ deg.

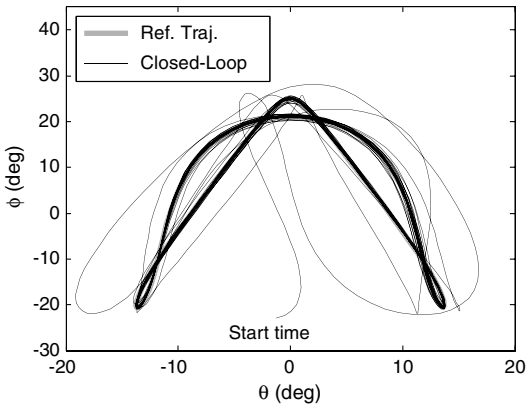

Fig. 11 Example of closed-loop control of tether librations under forced-current variations ($\bar{\varepsilon}_{\text{ref}} = 0.5 \cos \nu$, $k_1 = 1.5$, and $i = 25$ deg).

$i < 90$ deg for the current profile $\bar{\varepsilon} = 0.5 \cos \nu$. Note that all of these solutions appear linearly stable from the Floquet analysis.

The energy-rate feedback-controller stability was assessed for the inclination $i = 25$ deg, using k_1 as a continuation parameter. Figure 10 shows a contour plot of the maximum magnitude of the eigenvalues of the monodromy matrix. The plot shows that the controller yields a stable periodic solution, with the stability increasing with the magnitude of the control gain.

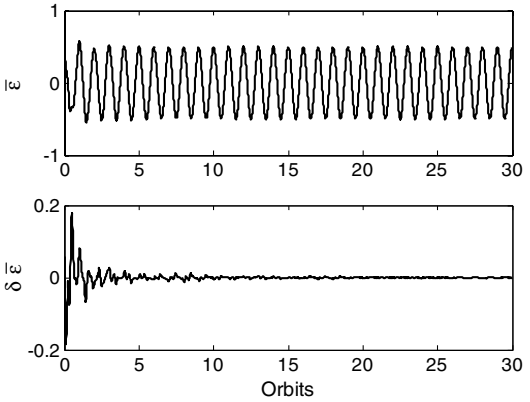

Fig. 12 Closed-loop control of tether librations under forced-current variations, showing a) total nondimensional current, and b) nondimensional current corrections due to feedback ($\bar{\varepsilon}_{\text{ref}} = 0.5 \cos \nu$, $k_1 = 1.5$, and $i = 25$ deg).

Figure 11 shows an example of the feedback controller using the reference current $\bar{\varepsilon} = 0.5 \cos \nu$ at an inclination of $i = 25$ deg and a control gain of $k_1 = 1.5$. A random initial perturbation is applied to the periodic solution in Fig. 11. The results illustrate faster convergence to the reference trajectory than for the case of a sinusoidal current input. Figure 12 shows the corresponding nondimensional current control input, illustrating that the control corrections are larger, but damp out faster, than in the previous case. The results show that the main disturbances are damped in approximately 10 orbits of the system.

C. Sinusoidal Input at Twice Orbital Frequency

Figure 13 shows the moduli of the eigenvalues of the monodromy matrix for a forced-current variation of the form $\bar{\varepsilon} = \varepsilon \sin 2\nu$ for an orbit inclination of 25 deg. Figure 13 shows that the system is mildly unstable for small current amplitudes, but appears to become linearly stable in the interval of $\varepsilon \approx (0.865, 1.35)$. Thus, it appears that certain families of forced currents can be linearly stable, as opposed to the case of a constant current, which always appears unstable. Above a value of $\varepsilon \approx 1.35$, the periodic solution becomes unstable again, and perturbations would move away more quickly from the periodic solution at these current levels. Figure 14 shows examples of the periodic solutions on the θ–ϕ phase plane for increasing values of ε. The shape of the periodic solution differs considerably from that shown in Figs. 2 and 8. The tip of the tether moves in a path resembling a figure eight. Increasing the value of the current increases the out-of-plane excursions of the tether and only moderately increases the peak-to-peak in-plane libration amplitude. The resulting periodic solution is symmetric in both the in- and out-of-plane directions. Figure 15 shows the effects of inclination on the moduli of the eigenvalues of the monodromy matrix for the case $\bar{\varepsilon} = 0.5 \sin 2\nu$. The periodic solutions appear to be linearly stable in the interval of $i \approx (36.5, 62.5)$ deg and $i \approx (115.5, 134.5)$ deg, whereas they are unstable outside of these intervals. Hence, it is clear that the stability of the periodic solutions under forced currents depends on the amplitude of the current, the forcing function, and the orbital inclination. Examples of the periodic solutions on the phase plane are shown in Fig. 16 for variations in the orbital inclination. All of these solutions are symmetric about two axes.

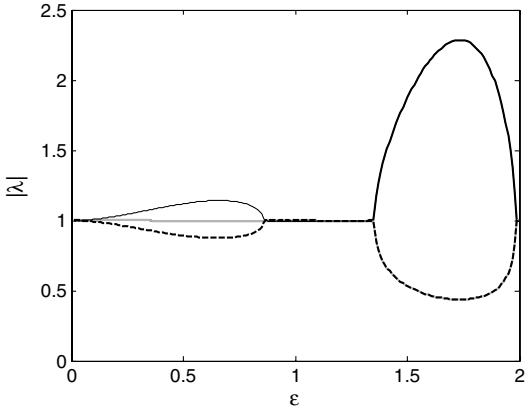

Fig. 13 Moduli of eigenvalues of monodromy matrix for $\bar{\varepsilon} = \varepsilon \sin 2\nu$, and $i = 25$ deg; λ_1 (thick black line), λ_2 (thin black line), λ_3 (thick gray line), and λ_4 (dashed line).

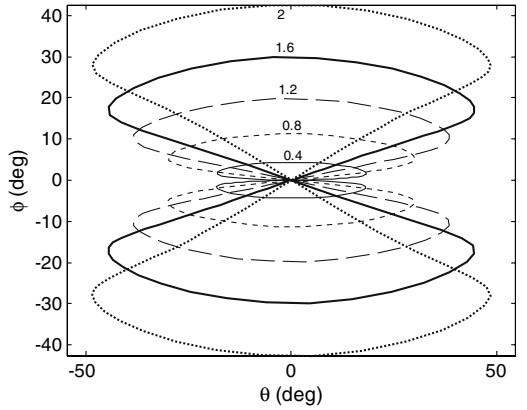

Fig. 14 Tether librations on phase plane for increasing ε for $\bar{\varepsilon} = \varepsilon \sin 2\nu$ and $i = 25$ deg (values of ε shown in plot).

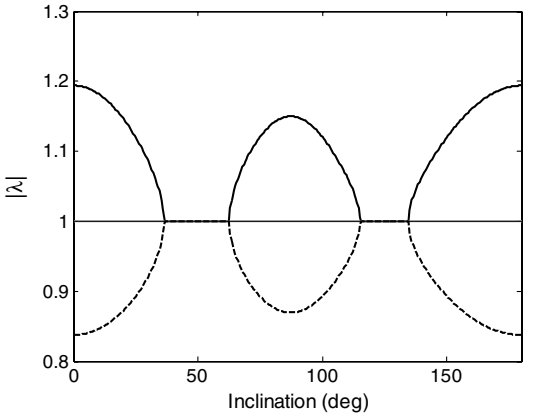

Fig. 15 Moduli of eigenvalues of monodromy matrix for $\bar{\varepsilon} = 0.5 \sin 2\nu$, and ($0 < i < 180$ deg); λ_1 (thick black line), λ_2 (thin black line), λ_3 (thick gray line), and λ_4 (dashed line).

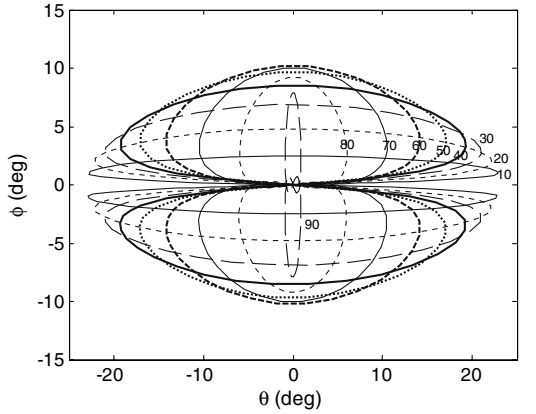

Fig. 16 Effect of inclination on $\bar{\varepsilon} = 0.5 \sin 2\nu$, shown at 10 deg increments $0 < i < 90$ deg (values of i shown in plot).

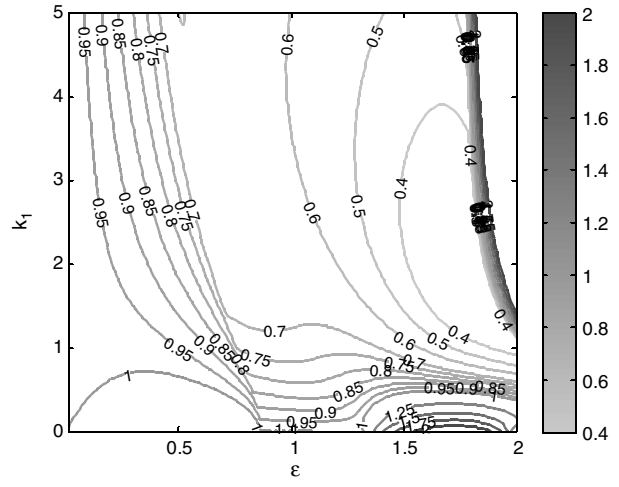

Fig. 17 Contours of maximum magnitude of the eigenvalues of the monodromy matrix for energy-rate feedback control with $\bar{\varepsilon} = \varepsilon \sin 2\nu$ and $i = 25$ deg.

The energy-rate feedback-controller stability was assessed for the inclination $i = 25$ deg, using k_1 as a continuation parameter. Figure 17 shows a contour plot of the maximum magnitude of the eigenvalues of the monodromy matrix. The plot shows that the feedback gain has a strong effect on the resulting controller stability. In particular, for sinusoidal and cosine variations at the orbital frequency, increasing the control gain leads to an increase in stability. However, for a sinusoidal input at twice the orbital frequency and for nondimensional current amplitudes greater than 1.35, the control gain must be greater than 0.5 for stability. However, when the nondimensional current amplitude exceeds 1.97, the controller becomes unstable for control gains exceeding 1.2.

Figure 18 shows a closed-loop simulation of the electrodynamic tether under a random initial disturbance away from the periodic solution. The case selected uses the reference current $\bar{\varepsilon} = 0.5 \sin 2\nu$ at an inclination of $i = 25$ deg and a control gain of $k_1 = 3$. This particular case is unstable in the absence of feedback. The simulation results demonstrate the convergence of the system trajectory to the periodic solution. The corresponding nondimensional current is shown in Fig. 19. The feedback current can be seen to be of relatively small magnitude, with a peak of approximately one-half of the forced-current amplitude. However, the total nondimensional current applied to the tether is not significantly affected by the feedback control, illustrating the excellent closed-loop performance of the controller. The errors decay in approximately five orbits.

D. Cosine Input at Twice Orbital Frequency

Figure 20 shows the moduli of the eigenvalues of the monodromy matrix for a forced-current variation of the form $\bar{\varepsilon} = \varepsilon \cos 2\nu$ for an orbit inclination of 25 deg. Figure 20 shows that the system is unstable for all current amplitudes, with the instability growing with current amplitude. Thus, it appears that both constant and cosine inputs at twice the orbital frequency lead to librational dynamics that are always unstable. These two current inputs are the two that are probably the most important for influencing the orbit (i.e., semimajor axis and inclination). Figure 21 shows examples of the periodic solutions on the θ–ϕ phase plane for increasing values of ε. The shape of the periodic solution resembles the periodic solutions for a constant current (see [8]), except that they are mirrored around the ϕ-axis. Increasing the value of the current increases both the in-plane and out-of-plane excursions of the tether. The resulting periodic

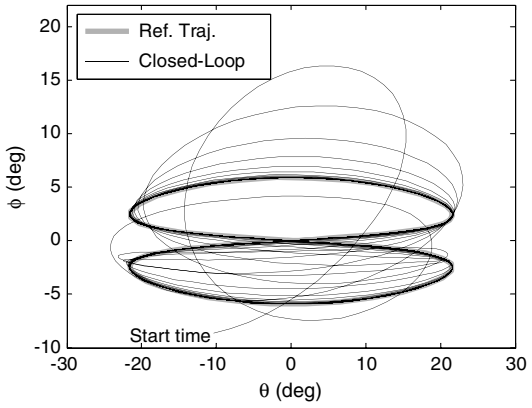

Fig. 18 Example of closed-loop control of tether librations under forced-current variations ($\bar{\varepsilon}_{\text{ref}} = 0.5 \sin 2\nu$, $k_1 = 3$, and $i = 25$ deg).

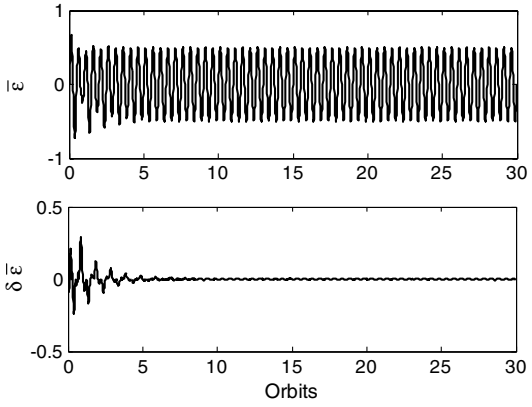

Fig. 19 Closed-loop control of tether librations under forced-current variations, showing a) total nondimensional current, and b) nondimensional current corrections due to feedback for $\bar{\varepsilon}_{\text{ref}} = 0.5 \sin 2\nu$, $k_1 = 3$, and $i = 25$ deg.

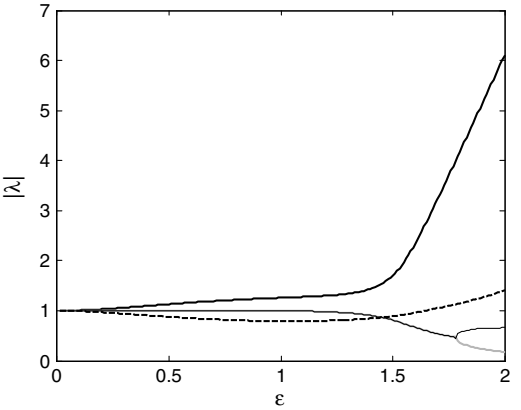

Fig. 20 Moduli of eigenvalues of monodromy matrix for $\bar{\varepsilon} = \varepsilon \cos 2\nu$, and $i = 25$ deg; λ_1 (thick black line), λ_2 (thin black line), λ_3 (thick gray line), and λ_4 (dashed line).

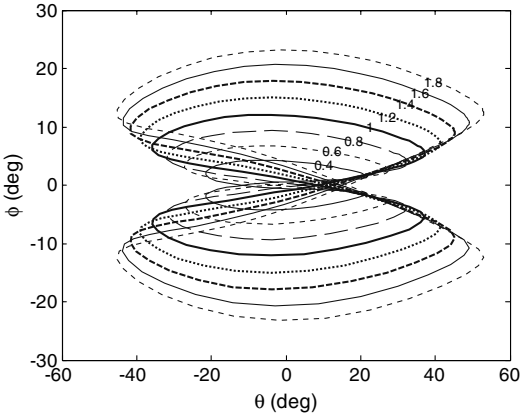

Fig. 21 Tether librations on phase plane for increasing ε for $\bar{\varepsilon} = \varepsilon \cos 2\nu$ and $i = 25$ deg (values of ε shown in plot).

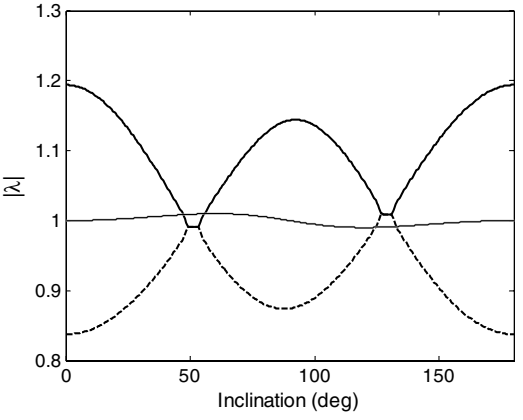

Fig. 22 Moduli of eigenvalues of monodromy matrix for $\bar{\varepsilon} = 0.5 \cos 2\nu$, and ($0 < i < 180$ deg); λ_1 (thick black line), λ_2 (thin black line), λ_3 (thick gray line), and λ_4 (dashed line).

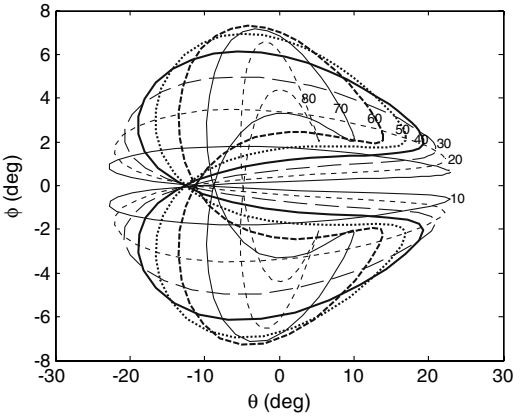

Fig. 23 Effect of inclination on $\bar{\varepsilon} = 0.5\cos 2\nu$, shown at 3 deg increments $0 < i < 90$ deg (values of i shown in plot).

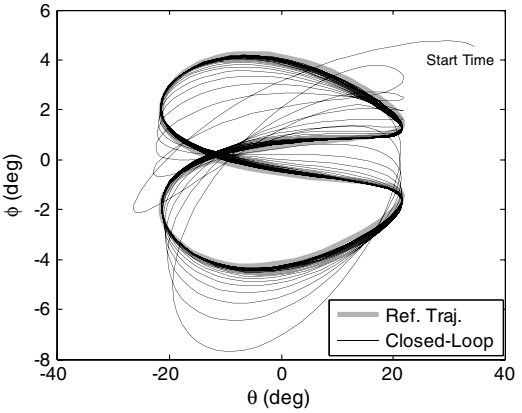

Fig. 25 Example of closed-loop control of tether librations under forced-current variations ($\bar{\varepsilon}_{\text{ref}} = 0.5\cos 2\nu$, $k_1 = 5$, and $i = 25$ deg).

solution is symmetric about the orbital plane. Figure 22 shows the effects of inclination on the moduli of the eigenvalues of the monodromy matrix for the case of $\bar{\varepsilon} = 0.5\sin 2\nu$. The periodic solutions appear to be unstable for all orbital inclinations, although the librations are only mildly unstable in the ranges of $51 < i < 75$ deg and $126.5 < i < 131$ deg. Examples of the periodic solutions on the phase plane are shown in Fig. 23 for variations in the orbital inclination. All of these solutions are symmetric about the orbital plane.

The energy-rate feedback-controller stability was assessed for the inclination $i = 25$ deg, using k_1 as a continuation parameter. Figure 24 shows a contour plot of the maximum magnitude of the eigenvalues of the monodromy matrix. The plot shows that over the range of control gains considered, there is a band of nondimensional amplitudes for which the feedback controller does not result in stable librations: $\varepsilon \approx (0.6, 1.4)$. Outside this range, it is possible to stabilize the librations using the energy-rate feedback controller.

Figure 25 shows a closed-loop simulation of the electrodynamic tether under a random initial disturbance away from the periodic solution. The case selected uses the reference current $\bar{\varepsilon} = 0.5\cos 2\nu$ at an inclination of $i = 25$ deg and a control gain of $k_1 = 5$. The simulation results demonstrate the convergence of the system trajectory to the periodic solution. The corresponding nondimensional current is shown in Fig. 26. The feedback current can be seen to be of relatively small magnitude, despite the larger gain compared with the previous closed-loop simulations. The significant errors decay in approximately 10 orbits, although convergence appears to be slower than for the previous simulations.

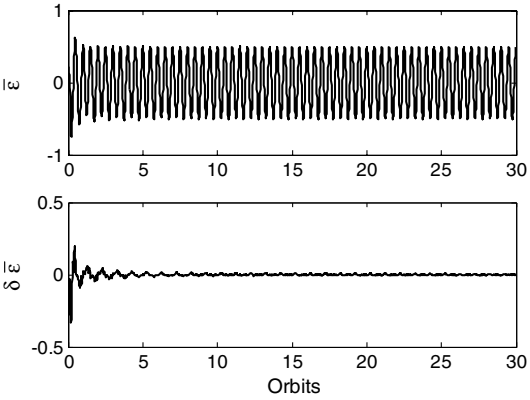

Fig. 26 Closed-loop control of tether librations under forced-current variations, showing a) total nondimensional current, and b) nondimensional current corrections due to feedback for $\bar{\varepsilon}_{\text{ref}} = 0.5\cos 2\nu$, $k_1 = 5$, and $i = 25$ deg.

E. Superposition of Constant-Current and Sinusoidal Input at Orbital Frequency

As a final example of a more practical scenario, the case of a forced current superimposed on a constant current is considered. This type of superposition is applicable in missions in which changes in one or more orbital elements are required simultaneously. Figure 27 shows the moduli of the eigenvalues of the monodromy matrix for the current profile $\bar{\varepsilon} = \varepsilon(1 + 0.5\sin 2\nu)$ for an inclination of $i = 25$ deg. This profile results in a current that is always positive.

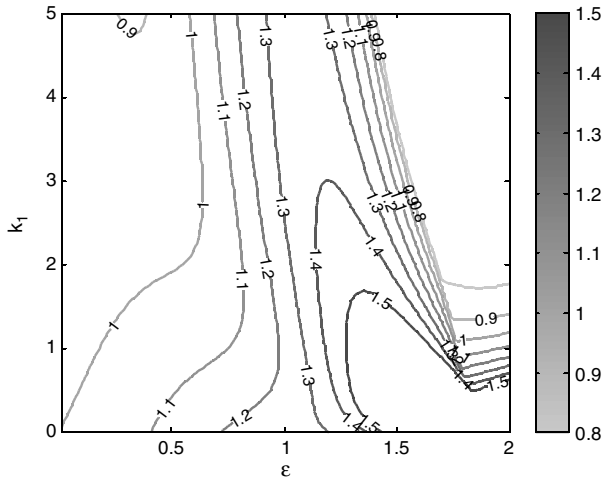

Fig. 24 Contours of maximum magnitude of the eigenvalues of the monodromy matrix for energy-rate feedback control with $\bar{\varepsilon} = \varepsilon\cos 2\nu$ and $i = 25$ deg.

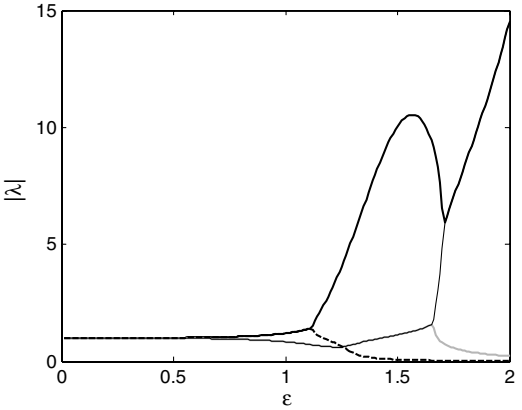

Fig. 27 Moduli of eigenvalues of monodromy matrix for $\bar{\varepsilon} = \varepsilon(1 + 0.5\sin 2\nu)$, and $i = 25$ deg; λ_1 (thick black line), λ_2 (thin black line), λ_3 (thick gray line), and λ_4 (dashed line).

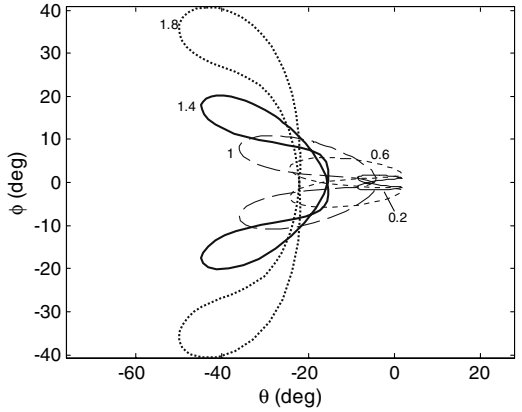

Fig. 28 Tether librations on phase plane for increasing ε for $\bar{\varepsilon} = \varepsilon(1 + 0.5\sin 2\nu)$ and $i = 25$ deg (values of ε shown in plot).

Figure 27 shows that the periodic solutions are only mildly unstable for small current amplitudes and become significantly more unstable for higher currents. The instability at higher currents appears to be larger than that observed for the case of a purely constant current [8], and the onset of significant instability occurs at lower mean current levels. This, however, is likely the consequence of the peak nondimensional currents being higher for this particular profile. Figure 28 shows examples of the periodic solutions on the phase plane for various values of ε for an inclination of $i = 25$ deg. The mean positive current value causes a steady-state offset of the in-plane tether libration angle, for which the value increases with ε. The effect of orbit inclination on the moduli of the eigenvalues of the monodromy matrix is shown in Fig. 29 for $\bar{\varepsilon} = 1.2(1 + 0.5\sin 2\nu)$.

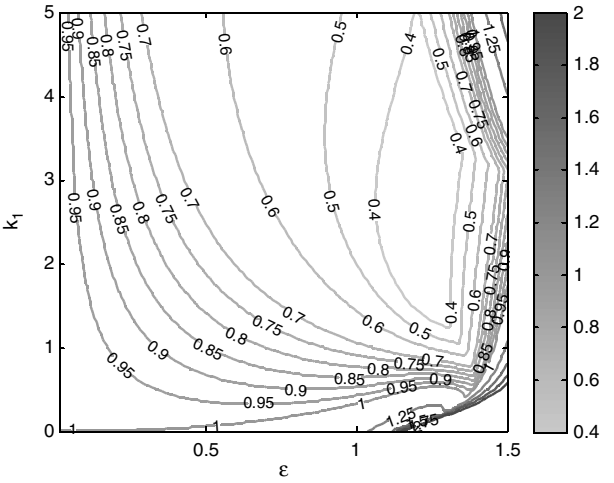

Fig. 31 Contours of maximum magnitude of the eigenvalues of the monodromy matrix for energy-rate feedback control with $\bar{\varepsilon} = \varepsilon(1 + 0.5\sin 2\nu)$ and $i = 25$ deg.

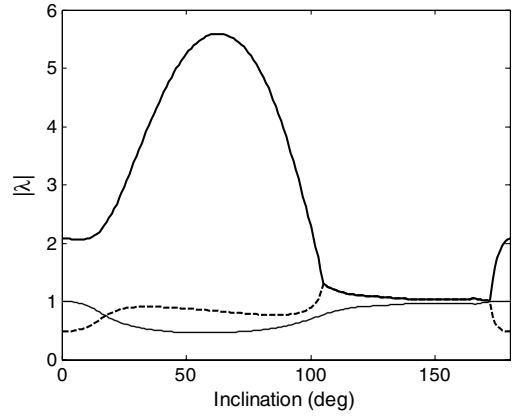

Fig. 29 Moduli of eigenvalues of monodromy matrix for $\bar{\varepsilon} = 1.2(1 + 0.5\sin 2\nu)$, and $(0 < i < 180$ deg); λ_1 (thick black line), λ_2 (thin black line), λ_3 (thick gray line), and λ_4 (dashed line).

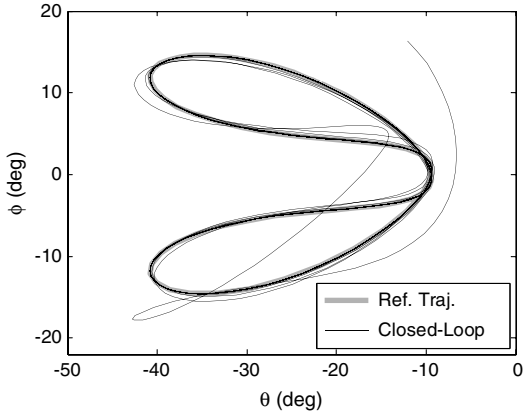

Fig. 32 Example of closed-loop control of tether librations under forced-current variations ($\bar{\varepsilon}_{\text{ref}} = 1.2(1 + 0.5\sin 2\nu)$, $k_1 = 3$, and $i = 25$ deg).

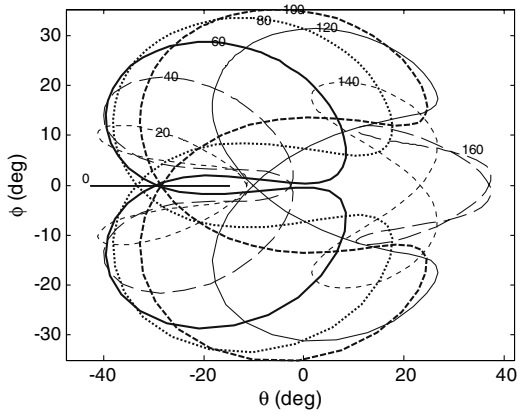

Fig. 30 Effect of inclination on $\bar{\varepsilon} = 1.2(1 + 0.5\sin 2\nu)$, shown at 3 deg increments $0 < i < 180$ deg (values of i shown in plot).

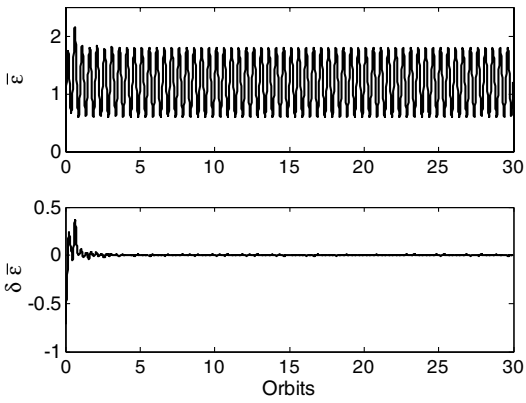

Fig. 33 Closed-loop control of tether librations under forced-current variations, showing a) total nondimensional current, and b) nondimensional current corrections due to feedback for $\bar{\varepsilon}_{\text{ref}} = 1.2(1 + 0.5\sin 2\nu)$, $k_1 = 3$, and $i = 25$ deg.

For very high inclinations between 108 and 168 deg (retrograde motion), the instability weakens considerably. Figure 30 shows examples of the periodic solutions on the phase plane. For $i = 0$, the periodic solution is one that remains in the orbital plane. As the inclination is increased, the out-of-plane component grows and the mean value of the in-plane librations decreases. Eventually, the mean value of the in-plane angle changes sign due to the change in orbit direction as the inclination passes through 90 deg. For $i = 180$ deg, the periodic solution is again in-plane only, but with a positive value of the in-plane angle.

The energy-rate feedback-controller stability was assessed for the inclination $i = 25$ deg, and Fig. 31 shows a surface plot of the maximum magnitude of the eigenvalues of the monodromy matrix. It is evident from this plot that the controller is able to stabilize the librations, but that there is only a narrow range of stable feedback gains for high values of ε. This is consistent with the results for a constant current given in [8].

The closed-loop performance of the system for the case $\bar{\varepsilon} = 1.2(1 + 0.5 \sin 2\nu)$ and $k_1 = 3$ at an inclination of 25 deg is shown in Fig. 32. The results show that the system is stabilized extremely well around the librational periodic solution. Figure 33 shows the corresponding nondimensional current and feedback current required to stabilize the trajectory. It can be seen that the system is stabilized in approximately three orbits and that the magnitude of the feedback current is relatively small. These examples demonstrate the possibilities of using forced-current variations for electrodynamic tethers and show the effectiveness of the feedback-control scheme for tracking the periodic solutions.

VII. Conclusions

Periodic solutions of electrodynamic tethers for case of forced-current variations were obtained and their stability properties were analyzed by means of Floquet's theory. A direct method based on the Legendre pseudospectral method was employed to obtain the solutions. The results indicate that, in contrast to the case of a constant current, some forced-current periodic solutions appear to be linearly stable. These are sinusoidal and cosine current inputs with frequencies equal to the orbital frequency and a sinusoidal input at twice the orbital frequency. Some regions of instability were obtained for different combinations of forcing currents, orbital inclination, and current amplitude. A cosine current at twice the orbital frequency is always unstable. A feedback-control approach for tracking the tether librational dynamics using additional current corrections was shown to work very well for the case of forced-current variations. Floquet analysis can be used to determine the range of control gains for which the closed-loop system is stable, and numerical simulations of closed-loop responses demonstrate closed-loop stability. When the reference current includes a constant component, the periodic solution is always unstable, requiring closed-loop control to stabilize the librations for long-term orbital maneuvers. Thus, most practical orbital maneuvering strategies involving changes to the orbit semimajor axis or orbit inclination result in unstable periodic librations.

Appendix: Application of Legendre Pseudospectral Method for Calculating Stability of Periodic Solutions

It will now be shown how the solution obtained via the Legendre pseudospectral method can be related to monodromy matrix [26].

Consider the discretization of Eq. (21) via the Legendre pseudospectral method,

$$\frac{1}{\xi}\sum_{j=0}^{N} D_{k,j}\delta\boldsymbol{x}_j - [\boldsymbol{A}(t_k)]\delta\boldsymbol{x}_k = \boldsymbol{0}, \qquad k = 0,\ldots,N, \qquad \delta\boldsymbol{x}_0 = \delta\boldsymbol{x}(0) \tag{A1}$$

which can be written in block matrix form as

$$[F]z = \begin{bmatrix} \frac{1}{\xi}\boldsymbol{D} - \boldsymbol{A}_{1,1} & -\boldsymbol{A}_{1,2} & \cdots & -\boldsymbol{A}_{1,n_x} \\ -\boldsymbol{A}_{2,1} & \frac{1}{\xi}\boldsymbol{D} - \boldsymbol{A}_{2,2} & \cdots & -\boldsymbol{A}_{2,n_x} \\ \vdots & \vdots & \vdots & \vdots \\ [1,0,\ldots,0] & \boldsymbol{0} & \cdots & \boldsymbol{0} \\ \boldsymbol{0} & [1,0,\ldots,0] & \cdots & \boldsymbol{0} \\ \vdots & \vdots & \ddots & \vdots \\ \boldsymbol{0} & \boldsymbol{0} & \cdots & [1,0,\ldots,0] \end{bmatrix} \begin{bmatrix} (\delta\widehat{x})_1 \\ (\delta\widehat{x})_2 \\ \vdots \\ (\delta\widehat{x})_{n_x} \end{bmatrix} = \begin{bmatrix} 0 \\ 0 \\ 0 \\ \delta\boldsymbol{x}(0) \end{bmatrix} \tag{A2}$$

where $\boldsymbol{A}_{k,j} = \mathrm{diag}[A_{k,j}(t_0),\ldots,A_{k,j}(t_N)]$ is a diagonal matrix that contains the entries of the variational equations at all LGL nodes evaluated on the periodic orbit, and

$$(\widehat{x})_j = [x_1, x_2, \ldots, x_N]_j \qquad j = 1,\ldots,n_x$$

(i.e., the values of the jth state at the LGL nodes). The matrix on the left-hand side of Eq. (A2), $[F]$, is nothing more than the Jacobian of the discretized constraints given in Eqs. (19) and (20) with respect to the states [note that a minor modification is necessary to set the derivatives of Eq. (20) with respect to $\boldsymbol{x}_N$ to zero]. The monodromy matrix can be formed in one of two ways. Equation (A2) can be solved n_x times with the appropriate initial conditions to obtain the values of the states at the final time $\delta\boldsymbol{x}_N$; alternatively, rearranging Eq. (A2) and eliminating the first row in each block of $[F]$ containing the differentiation matrix $\boldsymbol{D}$ renders the resulting $[F^*]$ matrix square with dimension $n_x(N+1)$. Assuming that the inverse of $[F^*]$ exists, let it be written as

$$[F^*]^{-1} = G \tag{A3}$$

Note that the existence of the inverse of $[F^*]$ cannot be guaranteed in general. In some situations, $[F^*]$ can become singular or nearly singular and it is necessary to use more accurate methods such as lower–upper decomposition to solve the system of equations. In other cases, it may be necessary to relax the equalities in Eq. (A2) to inequalities with a small tolerance. For more discussion on the existence of solutions via pseudospectral methods and the relaxation of equality constraints, see [37]. The monodromy matrix can be obtained by extracting the elements of G as follows:

$$M = \begin{bmatrix} G_{(N+1),1} & G_{(N+1),(N+1)+1} & \cdots & G_{(N+1),(n_x-1)(N+1)+1} \\ G_{2(N+1),1} & G_{2(N+1),(N+1)+1} & \cdots & G_{2(N+1),(n_x-1)(N+1)+1} \\ \vdots & \vdots & \vdots & \vdots \\ G_{n_x(N+1),1} & G_{n_x(N+1),(N+1)+1} & \cdots & G_{n_x(N+1),(n_x-1)(N+1)+1} \end{bmatrix} \tag{A4}$$

Equation (A4) relates the terminal values of the perturbed system in Eq. (21) to the initial conditions. Thus, the transformation is achieved without any explicit integration or additional analytic computations. The monodromy matrix can be formed directly from the Jacobian of the discretized nonlinear equations. The practical benefit of this is that virtually all nonlinear programming implementations compute the Jacobian. In this work, the software SNOPT [36] is used as the nonlinear programming solver. Another major benefit of this approach is that the Jacobian derivatives can be computed via finite differences. Thus, for highly complex systems in which analytic derivatives are difficult to compute, the method can be easily applied.

References

[1] Johnson, L., Estes, R. D., Lorenzini, E. C., Martinez-Sanchez, M., Sanmartin, J., and Vas, I., "Electrodynamic Tethers for Spacecraft Propulsion," AIAA Paper 98-0983, Jan. 1998.

[2] Johnson, L., and Herrmann, M., "International Space Station Electrodynamic Tether Reboost Study," NASA Marshall Space Flight Center TM-1998-208538, July 1998.

[3] Hoyt, R., "Tether Systems for Satellite Deployment and Disposal," 51st International Astronautical Congress, International Astronautical Federation, Paper 00-S.6.04, Oct. 2000.

[4] Forward, R. L., Hoyt, R. P., and Uphoff, C. W., "Terminator Tether: A Spacecraft Deorbit Device," *Journal of Spacecraft and Rockets*, Vol. 37, No. 2, 2000, pp. 187–196.
doi:10.2514/2.3565

[5] Gallagher, D. L., Johnson, L., Moore, J., and Bagenal, F., "Electrodynamic Tether Propulsion and Power Generation at Jupiter," NASA Marshall Space Flight Center TP-1998-208475, June 1998.

[6] Fujii, H. A., and Ichiki, W., "Nonlinear Dynamics of the Tethered Subsatellite System in the Station Keeping Phase," *Journal of Guidance, Control, and Dynamics*, Vol. 20, No. 2, 1997, pp. 403–406.
doi:10.2514/2.4057

[7] Peláez, J., Lorenzini, E. C., Lopez-Rebollal, O., and Ruiz, M., "A New Kind of Dynamic Instability in Electrodynamic Tethers," American Astronautical Society, Paper AAS 00-190.

[8] Williams, P., "Energy Rate Feedback for Libration Control of Electrodynamic Tethers," *Journal of Guidance, Control, and Dynamics*, Vol. 29, No. 1, 2006, pp. 221–223.
doi:10.2514/1.17530

[9] Peláez, J., and Lara, M., "Periodic Solutions in Electrodynamic Tethers on Inclined Orbits," *Journal of Guidance, Control, and Dynamics*, Vol. 26, No. 3, 2003, pp. 395–406.
doi:10.2514/2.5077

[10] Peláez, J., Ruiz, M., Lopez-Rebollal, O., Lorenzini, E. C., and Cosmo, M. L., "Two-Bar Model for the Dynamics and Stability of Electrodynamic Tethers," *Journal of Guidance, Control, and Dynamics*, Vol. 25, No. 6, 2002, pp. 1125–1135.
doi:10.2514/2.4992

[11] Peláez, J., and Andres, Y. N., "Dynamic Stability of Electrodynamic Tethers in Inclined Elliptical Orbits," *Journal of Guidance, Control, and Dynamics*, Vol. 28, No. 4, 2005, pp. 611–622.
doi:10.2514/1.6685

[12] Corsi, J., and Iess, L., "Stability and Control of Electrodynamic Tethers for De-Orbiting Applications," *Acta Astronautica*, Vol. 48, Nos. 5–12, 2001, pp. 491–501.
doi:10.1016/S0094-5765(01)00049-2

[13] Hoyt, R. P., "Stabilization of Electrodynamic Space Tethers," *Proceedings of Space Technology and Applications International Forum (STAIF-2002)*, American Inst. of Physics, Melville, NY, 2002, pp. 570–677.

[14] Williams, P., Blanksby, C., and Trivailo, P., "The Use of Electromagnetic Lorentz Forces as a Tether Control Actuator," *52nd International Astronautical Congress*, International Astronautical Federation, Paper 02-A.5.04, Oct. 2002.

[15] Netzer, E., and Kane, T. R., "Electrodynamic Forces in Tethered Satellite Systems, Part 1: System Control," *IEEE Transactions on Aerospace and Electronic Systems*, Vol. 30, No. 4, 1994, pp. 1031–1043.
doi:10.1109/7.328766

[16] Tani, J., and Qiu, J., "Motion Control of a Tethered Subsatellite Using Electromagnetic Force," *Proceedings of the Seventh International Conference on Adaptive Structures*, Technomic, Lancaster, PA, 1997, pp. 321–330.

[17] Williams, P., Watanabe, T., Blanksby, C., Trivailo, P., and Fujii, H. A., "Libration Control of Flexible Tethers Using Electromagnetic Forces and Movable Attachment," *Journal of Guidance, Control, and Dynamics*, Vol. 27, No. 5, 2004, pp. 882–897.
doi:10.2514/1.1895

[18] Takeichi, N., "Libration Control of an Electrodynamic Tethered System Through Electric Current Switching," AAS/AIAA Astrodynamics Specialists Conference, Lake Tahoe, NV, American Astronautical Society, Paper 05-318, Aug. 2005.

[19] Lanoix, E., Misra, A., Modi, V., and Tyc, G., "Effect of Electromagnetic Forces on the Orbital Dynamics of Tethered Satellites," *Journal of Guidance, Control, and Dynamics*, Vol. 28, No. 6, 2005, pp. 1309–1315.
doi:10.2514/1.1759

[20] Peláez, J., and Lorenzini, E. C., "Libration Control of Electrodynamic Tethers in Inclined Orbit," *Journal of Guidance, Control, and Dynamics*, Vol. 28, No. 2, 2005, pp. 269–279.
doi:10.2514/1.6473

[21] Williams, P., "Librational Stabilization of Electrodynamic Tethers Using Time-Delayed Predictive Control," *Journal of Guidance, Control, and Dynamics*, Vol. 32, No. 4, 2009, pp. 1254–1268.
doi:10.2514/1.41039

[22] Tragesser, S. G., and San, H., "Orbital Maneuvering with Electrodynamic Tethers," *Journal of Guidance, Control, and Dynamics*, Vol. 26, No. 5, 2003, pp. 805–810.
doi:10.2514/2.5115

[23] Williams, P., "Simple Approach to Orbital Control using Spinning Electrodynamic Tethers," *Journal of Spacecraft and Rockets*, Vol. 43, No. 1, 2006, pp. 253–256.
doi:10.2514/1.16608

[24] Sabey, N., and Tragesser, S., "Effects of Libration on General Electrodynamic Tether Orbital Maneuvers," *AIAA/AAS Astrodynamics Specialist Conference*, AIAA Paper 2008-7510, Aug. 2008.

[25] Lara, M., and Peláez, J., "On the Numerical Continuation of Periodic Orbits: An Intrinsic, 3-Dimensional, Differential, Predictor-Corrector Algorithm," *Astronomy and Astrophysics*, Vol. 389, No. 2, 2002, pp. 692–701.
doi:10.1051/0004-6361:20020598

[26] Williams, P., "Direct Numerical Computation of Periodic Orbits and Their Stability," *Journal of Spacecraft and Rockets*, Vol. 43, No. 5, 2006, pp. 1143–1146.
doi:10.2514/1.20930

[27] Williams, P., "Electrodynamic Tethers Under Forced-Current Variations Part 2: Flexible-Tether Estimation and Control," *Journal of Spacecraft and Rockets*, Vol. 47, No. 2, 2009, pp. 320–333.
doi:10.2514/1.45733

[28] Carroll, J. A., *Guidebook for Analysis of Tether Applications*, NASA, March 1985.

[29] Elnagar, J., Kazemi, M. A., and Razzaghi, M., "The Pseudospectral Legendre Method for Discretizing Optimal Control Problems," *IEEE Transactions on Automatic Control*, Vol. 40, No. 10, 1995, pp. 1793–1796.
doi:10.1109/9.467672

[30] Ross, I. M., and Fahroo, F., "Legendre Pseudospectral Approximations of Optimal Control Problems," *Lecture Notes in Control and Information Sciences*, Vol. 295, Springer–Verlag, New York, pp. 327–342.

[31] Ross, I. M., King, J. T., and Fahroo, F., "Designing Optimal Spacecraft Formations," AIAA Paper 2002-4635, Aug. 2002.

[32] Infeld, S. I., Josselyn, S. B., Murray, W., and Ross, I. M., "Design and Control of Libration Point Spacecraft Formations," AIAA Paper 2004-4786.

[33] Williams, P., "Libration Control of Tethered Satellites in Elliptical Orbits," *Journal of Spacecraft and Rockets*, Vol. 43, No. 2, 2006, pp. 476–479.
doi:10.2514/1.17499

[34] Gong, Q., Ross, I. M., Kang, W., and Fahroo, F., "Convergence of Pseudospectral Methods for Constrained Nonlinear Optimal Control Problems," *Intelligent Systems and Control*, Series on Modelling, Identification and Control, Acta Press, Calgary, Canada, 2004.

[35] Meirovitch, L., *Methods of Analytical Dynamics*, McGraw–Hill, New York, 1970, Chap. 7.

[36] Gill, P. E., Murray, W., and Saunders, M. A., "SNOPT: An SQP Algorithm for Large-Scale Constrained Optimization," *SIAM Journal on Optimization*, Vol. 12, No. 4, 2002, pp. 979–1006.
doi:10.1137/S1052623499350013

[37] Gong, Q., Ross, I. M., Kang, W., and Fahroo, F., "Dual Convergence of the Legendre Pseudospectral Method for Solving Nonlinear Constrained Optimal Control Problems," *Proceedings of the Intelligent Systems and Control Conference*, Univelt, San Diego, CA, Nov. 2005, Paper 497-110.

C. Kluever
Associate Editor